Metabolic effects of air pollution exposure and reversibility

Sanjay Rajagopalan[a,d*†], Bongsoo Park[b†], Rengasamy Palanivel[a], Vinesh Vinayachandran[a], Jeffrey A. Deiuliis[a], Roopesh Singh Gangwar[a], Lopa Das[a], Jinhu Yin[b], Youngshim Choi[b], Sadeer Al-Kindi[a], Mukesh K. Jain[a,d], Kasper D. Hansen[c] and Shyam Biswal[b*]

[a] Cardiovascular Research Institute, Case Western Reserve University, Cleveland, OH 44106, USA; [b] Department of Environmental Health and Engineering; [c] Department of Biostatistics, Johns Hopkins Bloomberg School of Public Health, Johns Hopkins University, Baltimore, MD 21205, USA; [d] Harrington Heart and Vascular Institute, University Hospital Cleveland Medical Center, Cleveland, OH 44106, USA.

†Contributed equally as first author.

*Correspondence to Sanjay Rajagopalan: sxr647@case.edu, Shyam Biswal: sbiswal1@jhu.edu

Classification

Biological Sciences, Environmental Sciences

Keywords

Air pollution, $PM_{2.5}$, Transcriptome, Insulin Resistance, Epigenome

Conflict of interest statement

The authors have declared that no conflict of interest exists.

Abstract

Particulate matter < 2.5 micrometers ($PM_{2.5}$) air pollution is the world's leading environmental risk factor contributing to mortality through cardiometabolic pathways. In this study, we modeled early life exposure using chow-fed C57BL/6J male mice, exposed to real-world inhaled concentrated $PM_{2.5}$ (~10 times ambient levels / ~60-120$\mu g/m^3$) or filtered air over 14 weeks. We investigated $PM_{2.5}$ effects on phenotype, transcriptome and chromatin accessibility, compared the effects with a prototypical high-fat diet (HFD) stimulus, and examined cessation of exposure on reversibility of phenotype. Exposure to $PM_{2.5}$ impaired glucose and insulin tolerance, reduced energy expenditure and ^{18}FDG-PET uptake in brown adipose tissue. Multiple differentially expressed gene (DEG) clusters in pathways involving metabolism and circadian rhythm were noted in insulin responsive tissues. Although the magnitude of transcriptional change seen with $PM_{2.5}$ was lower than HFD, the degree of alteration in chromatin accessibility after $PM_{2.5}$ exposure was significant. A novel chromatin remodeler SMARCA5 (SWI/SNF complex) was regulated in response to $PM_{2.5}$ with cessation of exposure associated with reversal of insulin resistance, restoration of chromatin accessibility/nucleosome positioning near transcription start sites (TSS) and exposure induced changes in the transcriptome including SMARCA5, indicating pliable epigenetic control mechanisms following exposure cessation.

Introduction

Air pollution is the leading environmental cause of premature reversible death and disability in the world today (1). A large body of evidence implicates the particulate matter <2.5 micron ($PM_{2.5}$) component of air pollution in the development of risk factors for cardiovascular disease such as hypertension and insulin resistance (IR) and type 2 diabetes mellitus (T2DM) (2, 3). Although the mechanisms by which inhalation of $PM_{2.5}$ induces IR and T2DM remain unclear, a constellation of responses including inflammation, and redox stress, have been implicated. There have been no previous studies that have examined metabolic, transcriptomic, and epigenetic effects of air pollution in comparison with other stressors such as high-fat diet (HFD). Importantly, the reversibility of $PM_{2.5}$-induced transcriptional and epigenetic changes has not been examined. In this study, we evaluated the metabolic phenotypic, transcriptional, and epigenomic changes in response to exposure to concentrated ambient $PM_{2.5}$ and the response of these parameters to cessation of exposure.

Results and Discussion

Air Pollution Exposure

C57BL/6J mice at 3 weeks receiving chow diet began concentrated ambient $PM_{2.5}$ exposure ($PM_{2.5}$ in the rest of the manuscript) for 14 weeks. Figure 1 is a summary of the systemic effects of ambient air pollution on IR from $PM_{2.5}$-exposed male mice. $PM_{2.5}$ was delivered inhalationally (~10x ambient level/~60-120μg/m^3) for 6 hours/day, 5 days/week) using a Versatile Aerosol Concentrator and Enrichment System [Fig. S1 provides $PM_{2.5}$ concentrations during the exposure period (mean $PM_{2.5}$ concentration was 80 μg/m^3, ~10x ambient concentration), meteorological conditions and elemental characterization of air pollution exposure]. Three-week old, C57BL/6J mice were fed a HFD for 14 weeks and served as a positive control for IR and associated transcriptomic and epigenomic changes.

Insulin Resistance and Metabolic Dysfunction with Air Pollution exposure

$PM_{2.5}$ exposure resulted in alterations in glucose clearance compared to filtered air (FA) in males. Insulin responsiveness (Fig. 1B-C) was also altered by $PM_{2.5}$ exposure. No difference in mean group body weight was observed (Fig. S2A). Metabolic cage experiments demonstrated reduction in VO_2, VCO_2, and Energy Expenditure (EE) in $PM_{2.5}$-exposed mice, during both light (ZT 0-12) and dark phases (ZT 12-24) (Fig. 1D-F). $PM_{2.5}$ exposure reduced Respiratory Quotient at nighttime alone (Fig. S2D). $PM_{2.5}$ exposed mice had reduced glucose uptake in brown adipose tissue (BAT) as measured by ^{18}FDG positron emission tomography (PET) (Fig. 1G). Body mass increased in response to HFD but not with $PM_{2.5}$ in both males and females (Fig. S2A). $PM_{2.5}$ induced abnormalities in glucose clearance and insulin responses that were comparable to HFD but were seen only in males (Fig. S2B-C). Given that phenotypic changes were seen only in males, we restricted further analysis to males. We acknowledge that is entirely possible that there could still be conserved responses in males and females that diverge from the sexual dimorphic responses of glucose tolerance and insulin responsiveness. Hepatic cholesterol but not plasma cholesterol increased in the $PM_{2.5}$ group, while lipid deposition and fibrosis were increased in both $PM_{2.5}$- and

HFD-exposed mice (Fig. S3A, B). Hepatic inflammation in $PM_{2.5}$ and HFD was characterized by an elevation of "pro-inflammatory" M1 genes (TNF-a, IL-6, and TLR4) and downregulation of anti-inflammatory "M2" genes (IL-10; Fig S3C-D). Liver adiponectin was markedly downregulated in response to $PM_{2.5}$ exposure. In many of these genes, the degree of regulation and directionality in hepatic tissue was comparable to HFD (Fig. S3C-D). Hepatic glycogen was decreased in $PM_{2.5}$, albeit to a lesser degree *vs.* HFD (Fig. S3E).

In summary, the phenotype encountered with chronic air pollution exposure was characterized by alterations in oxygen consumption and EE, hepatic inflammation, elevated triglycerides with evidence of hepatic steatosis and glycogen depletion. Interestingly, mice exposed to air-pollution do not develop adiposity, similar to the phenotype of lean IR, common in many parts of Asia. Importantly, we demonstrated a strong sexual dimorphic response with only males developing IR.

Differential Transcriptome and Functional Annotation of $PM_{2.5}$ vs. HFD Exposure

Transcriptomes were quantified using RNA-sequencing of RNA from liver, skeletal muscle, brown adipose, white adipose and hypothalamus from FA and $PM_{2.5}$ mice, which resulted in the identification of multiple differentially expressed genes (DEGs; Fig. 2A). Supplemental Figure S4A-F shows results of our principal component analysis (PCA) according to tissue of origin and exposure status. In summary, a total of 589 DEGs were discovered for $PM_{2.5}$ exposure versus FA, with 11 genes being differentially expressed in 2 tissue types (Venn diagram, Fig. 2A). The high-fat diet appeared to induce large transcriptional changes across all tissue types (Fig. 2B). In contrast, $PM_{2.5}$ changes were less pronounced with the largest number of DEGs in brown adipose tissue (BAT), followed by white adipose tissue (WAT) and liver (Fig. 2B). The most enriched of GO terms in $PM_{2.5}$ were related to cancer progression, cardiometabolic function and circadian rhythm and corresponding pathways associated with these were inflammation, redox stress, metal ion transport, and glucose metabolism (Fig. 2C). In contrast, HFD induced changes in fatty acid biosynthesis, inflammation, gluconeogenesis and lipid regulatory pathways. More detailed DEGs,

functional annotations, and potential up-stream and downstream regulators are summarized in the data supplement (Fig. S5-9). Figure S4G depicts the number and directionality of DEGs in response to $PM_{2.5}$ and HFD when compared with FA. In liver, WAT, hypothalamus, and muscle the number of DEGs that were concordant was higher than genes displaying a discordant response. BAT had a comparable number of DEGs that were discordant as were concordant (Fig S4G).

Differentially Expressed Genes in Insulin Responsive Tissue and Functional Annotations

$PM_{2.5}$-induced 42 DEGs in the liver, of which 35 overlapped with HFD-induced DEGs (S4G). Gene Ontology (GO) showed that circadian rhythm genes in the liver ranked at the top of the analysis (GO:0007623 circadian rhythms). These included transcriptional regulators (*eg.* Dbp, Bhlhe41, Cry1, Per3 and Arntl/Bmal1). While core clock components Cryptochrome 1 (Cry1), and Bmal1 (Arntl1) were downregulated with $PM_{2.5}$, the transcriptional repressor, Basic helix-loop-helix family member e41 (Bhlhe41) was upregulated (4). Ppp1r3g a markedly downregulated gene with $PM_{2.5}$ exposure belongs to a family of glycogen-targeting regulatory subunits (G subunits) that coordinate glycogen synthesis, by targeting the catalytic subunit of PP1 to the glycogen particles, and activate Glycogen Synthase through PP1-mediated dephosphorylation (5). These findings were consistent with glycogen depletion in response to $PM_{2.5}$ exposure (Fig. S3D). Several G protein receptor proteins (C5ar1, Celsr1, Adgrv1) were downregulated in the liver including the nuclear receptor protein Nr4a1 (Nur77) (Fig. 2D). Previous studies have identified Nr4a1 as a transcriptional regulator of glucose utilization in liver and macrophage polarization (6, 7). Rgs16, a regulator of G protein signaling shown to restrict the pro-inflammatory response of monocytes, was the most upregulated gene in the liver (8). In addition, Figure S7E depicts TGF-β signaling pathway and the corresponding DEGs in $PM_{2.5}$ and HFD. We also observed the downregulation of mTOR signaling DEGs (Fig. S8A, FDR<0.1). The enriched functional pathways and diseases for skeletal muscle and hypothalamus are summarized in Figure S9. BAT, WAT and liver tissues demonstrated the most overlapping DEGs between $PM_{2.5}$ and HFD exposures (Fig. S4G). In contrast, skeletal muscle and hypothalamus demonstrated smaller number of common DEGs in response to HFD and $PM_{2.5}$.

Enriched pathway terms specific for BAT DEGs upregulated specifically with $PM_{2.5}$, included T2DM signaling and nNOS signaling (Fig. S5B). We also observed the downregulation of adipogenesis DEGs (Ccng2, Acly, Slc25a1, Angptl4) and upregulation of inflammatory response DEGs from gene set enrichment analysis in BAT (Fig. S5C). Ppp1r3b (Protein Phosphatase 1 Regulatory Subunit 3G) in BAT an analogue of Ppp1r3g, was markedly downregulated with both $PM_{2.5}$ and HFD (Fig. 2D), while Mstn (Myostatin), known to be linked to diabetes (9), was markedly upregulated in BAT (Fig. 2D). Figure S6 depicts functional links between upregulated genes in WAT and corresponding pathways.

Our results support epidemiologic and empirical observations linking air pollution with pathways that promote susceptibility to other non-communicable diseases (1-3). Circadian rhythm alterations constitute a common denominator for the development of cancer, metabolic and cardiovascular disease (10-12). Many circadian factors are classic epigenetic regulators and conversely many metabolites impact epigenetic regulators and the epigenomic landscape (13, 14).

Changes in Chromatin Accessibility in Response to $PM_{2.5}$ and HFD

Given that $PM_{2.5}$ exposure resulted in a distinct transcriptomic response (Fig. 3A) with similarities to HFD, we hypothesized that DEGs may be regulated by epigenetic reprogramming driven by differential transcription factor binding. Using ATAC-Seq, we evaluated genome-wide chromatin accessibility in the liver of exposed mice and compared them with HFD (Fig. 3B). We analyzed the ATAC-Seq datasets based on the fragment size distribution, according to fragment sizes and identified uniquely reproducible peaks in $PM_{2.5}$ and HFD groups (Fig. S11A-B). We further identified differentially accessible regions (DARs), and 218 regions were common gain-of-accessibility, and 124 regions were common loss of accessibility (Fig. S11C). We also explored the degree of concordance/discordance between transcriptomic and epigenomic alterations in response to HFD and $PM_{2.5}$ (Fig. 3B-C). The DARs generally corresponded with upregulated gene expression and conversely less accessible regions with downregulated gene expression. We summarized the GC/AT ratio on the promoter sites (Fig. 3B) as a reflection of chromatin accessibility, corresponding

to CpG rich regions. Out of the reproducible peaks that overlapped with both FA and $PM_{2.5}$, 1,937 peaks were differentially accessible with $PM_{2.5}$ exposure (Fig. S11C). Among those peaks, we searched for $PM_{2.5}$ specific differential "distal" peaks, denoting potential distal regulatory sites (1-5k, 10k, 25k, 100k, 500k and >500k, Figure 3C) and performed differential motif binding analysis (15) using publicly available ChIP-Seq datasets (16). We found the chromatin remodeler SMARCA5 (SWI/SNF-Related Matrix-Associated Actin-Dependent Regulator of Chromatin Subfamily A Member 5) to be a differential binding protein in $PM_{2.5}$-exposed mice when compared to FA (Fig. 3D-E).

Epigenetic reprogramming in response to environmental exposure may represent a critical buffer against adverse health response through regulation of gene expression and chromosome integrity (17). Circadian rhythm genes in the liver ranked at the top of gene ontology analysis in our study, with changes in core clock components and transcriptional regulators of circadian rhythm. While the core clock components Cryptochrome 1 (Cry1), and Bmal1 (Arntl1) were downregulated in response to $PM_{2.5}$, the transcriptional repressor of the Clock-Arntl/Bmal1 heterodimer, Basic helix-loop-helix family member e41 (Bhlhe41) was upregulated.

Cessation of $PM_{2.5}$ exposure leads to reversal in transcriptomic and epigenomic changes

Eight weeks of cessation showed improvement in glucose tolerance and insulin sensitivity (Fig. 4A). Given the degree of phenotypic variation in reversibility (Fig. S12A-B), we were interested in corresponding transcriptomic and epigenomic changes. Figure 4B depicts reversal of a number of highly regulated genes in liver and WAT, suggesting marked reversibility within 8 weeks of exposure cessation (Fig. 4C, S13). We performed ATAC-Seq on liver to identify possible chromatin accessibility changes, as a reversal mechanism after cessation of $PM_{2.5}$ exposure. Figure S14A depicts DARs in response to $PM_{2.5}$ cessation in liver. In total, we discovered 3,467 DARs that changed in the liver following $PM_{2.5}$ cessation. Analysis of the regulatory elements of the same DARs showed that cis-regulatory regions that change with cessation are highly enriched in pathways related to insulin action, resistance, gluconeogenesis and metabolism (Fig. S14B).

Figure S14C depicts protein-genes (N=21,955) as a heatmap of all proximal peaks (± 1kb) from TSS, depicting changes in chromatin accessibility following reversal. Interestingly, SMARCA5 that was shown to be regulated in response to $PM_{2.5}$ demonstrated reversibility with cessation (Fig. 4D). Two of the most highly regulated genes in the liver were Nr4a1 (Nur77) and Rgs16 genes, which happen to be particularly relevant to the genesis of IR and inflammation (6, 18). The impact of cessation on the expression and regulatory elements of the most upregulated (Rgs16) and downregulated genes (Nr4a1) in the liver is depicted in Figure 4E and F. Epigenomic changes with exposure cessation were concordant with the change in mRNA for a number of circadian genes, providing evidence for transcription reprogramming in their promoter (*eg.* Rgs16 promoter, Fig. S13B) and Bmal1 promoter (Fig. S15). Reversible changes in circadian genes seen with cessation of exposure suggest causality of air pollution exposure in circadian dysregulation.

$PM_{2.5}$ promoted significant chromatin remodeling, especially in promoter and enhancer sites that were pliable, with cessation of exposure, resulting in reversal of changes in chromatin accessibility and transcript notably for genes involved in insulin action, circadian rhythm, and inflammation. An important additional finding was that SMARCA5 (SWI/SNF complex) was regulated in response to $PM_{2.5}$ and was reversible with cessation. SWI/SNF complexes are a family of polymorphic ATP-dependent chromatin remodeling complexes that are recruited to *cis*-regulatory elements such as promoters and enhancers, where they contribute to chromatin accessibility (19). Chromatin remodeling may be particularly important in the context of environmental exposures where epigenomic changes may be required to buffer and regulate gene expression (17). A growing body of evidence shows that long- and short-term exposure to ambient $PM_{2.5}$ are associated with altered DNA methylation in specific genes in relation to inflammation, vascular endothelial dysfunction and cytokines, with these effects implicated in perturbation of circulating cytokines, and fasting blood glucose (20-22).

Our study has limitations that must be acknowledged. We did not identify the precise epigenetic regulators that lead to metabolic dysfunction through genome-wide methylation analysis. In addition, histone modifications (*e.g.* H3K36me3, activation marks; H3K27me3,

repression marks; H3K27ac, enhancer marks) and the 3D structure of the chromatin may be also involved in epigenetic reprogramming upon chronic $PM_{2.5}$ exposure. Our results will need validation in well-designed human studies and if confirmed, may have important implications for interventions to reduce air pollution levels and exposure.

Methods

See Supplemental Material for Methods. All animal procedures and experiments were approved by the IACUC committee (Case Western Reserve University, OH) before they were undertaken.

Data availability: Sequencing data from this study have been submitted to the NCBI Gene Expression Omnibus (GEO; http://www.ncbi.nlm.nih.gov/geo/) under accession number GSE145840.

Author Contributions

SR and SB conceptualized and initiated study, edited and approved the final manuscript. BP wrote a draft manuscript. BP and KDH conducted bioinformatics analysis and created most figures. PR, RSG, XR, and YC conducted $PM_{2.5}$ exposure and tissue collection. PR conducted phenotype assays including liver histology, microscope imaging, and GTT/ITT. JD conducted analysis and edited manuscript. JY supported DNA/RNA preparation and conducted the qPCR assay. VV prepared preparation of sequencing libraries and performed OMNI ATAC-Seq. SAK and MKJ reviewed the manuscript and provided critical comments. All authors are contributed to revise and finalize manuscripts.

Acknowledgments

We appreciate the helping from Adele Snowman, Bindu Paul and Lie Gao regarding whole brain dissection, and Juhyung Woo, and Justin Edwards regarding tissue collection. Authors thank Alexias Safi and Gregory Crawford at Duke University to perform ATAC-Seq using original protocol for liver samples. Authors thank Justin Colacino and Judith S. Opp for transcriptome sequencing at University of Michigan. This work was supported by NIEHS U01ES026721 to SB and SR and R01ES015146 R01ES019616 to SR.

References

1. Landrigan PJ, Fuller R, Acosta NJR, Adeyi O, Arnold R, Basu NN, et al. The Lancet Commission on pollution and health. *Lancet.* 2018;391(10119):462-512.
2. Munzel T, Sorensen M, Gori T, Schmidt FP, Rao X, Brook FR, et al. Environmental stressors and cardio-metabolic disease: part II-mechanistic insights. *Eur Heart J.* 2017;38(8):557-64.
3. Rajagopalan S, Al-Kindi SG, and Brook RD. Air Pollution and Cardiovascular Disease: JACC State-of-the-Art Review. *Journal of the American College of Cardiology.* 2018;72(17):2054-70.
4. Sato F, Kohsaka A, Bhawal UK, and Muragaki Y. Potential Roles of Dec and Bmal1 Genes in Interconnecting Circadian Clock and Energy Metabolism. *Int J Mol Sci.* 2018;19(3).
5. Agius L. Glucokinase and molecular aspects of liver glycogen metabolism. *Biochem J.* 2008;414(1):1-18.
6. Chao LC, Wroblewski K, Zhang Z, Pei L, Vergnes L, Ilkayeva OR, et al. Insulin resistance and altered systemic glucose metabolism in mice lacking Nur77. *Diabetes.* 2009;58(12):2788-96.
7. Shaked I, Hanna RN, Shaked H, Chodaczek G, Nowyhed HN, Tweet G, et al. Transcription factor Nr4a1 couples sympathetic and inflammatory cues in CNS-recruited macrophages to limit neuroinflammation. *Nature immunology.* 2015;16(12):1228-34.
8. Suurvali J, Pahtma M, Saar R, Paalme V, Nutt A, Tiivel T, et al. RGS16 restricts the pro-inflammatory response of monocytes. *Scand J Immunol.* 2015;81(1):23-30.
9. Guo T, Bond ND, Jou W, Gavrilova O, Portas J, and McPherron AC. Myostatin inhibition prevents diabetes and hyperphagia in a mouse model of lipodystrophy. *Diabetes.* 2012;61(10):2414-23.
10. Crnko S, Du Pre BC, Sluijter JPG, and Van Laake LW. Circadian rhythms and the molecular clock in cardiovascular biology and disease. *Nat Rev Cardiol.* 2019.

11. Bass J, and Lazar MA. Circadian time signatures of fitness and disease. *Science.* 2016;354(6315):994-9.

12. Takahashi JS. Transcriptional architecture of the mammalian circadian clock. *Nat Rev Genet.* 2017;18(3):164-79.

13. Masri S, Zocchi L, Katada S, Mora E, and Sassone-Corsi P. The circadian clock transcriptional complex: metabolic feedback intersects with epigenetic control. *Ann N Y Acad Sci.* 2012;1264:103-9.

14. Masri S, and Sassone-Corsi P. The circadian clock: a framework linking metabolism, epigenetics and neuronal function. *Nat Rev Neurosci.* 2013;14(1):69-75.

15. Tripodi IJ, Allen MA, and Dowell RD. Detecting Differential Transcription Factor Activity from ATAC-Seq Data. *Molecules.* 2018;23(5).

16. Kulakovskiy IV, Vorontsov IE, Yevshin IS, Sharipov RN, Fedorova AD, Rumynskiy EI, et al. HOCOMOCO: towards a complete collection of transcription factor binding models for human and mouse via large-scale ChIP-Seq analysis. *Nucleic Acids Res.* 2018;46(D1):D252-D9.

17. Padmanabhan K, and Billaud M. Desynchronization of Circadian Clocks in Cancer: A Metabolic and Epigenetic Connection. *Front Endocrinol (Lausanne).* 2017;8:136.

18. Vivot K, Moulle VS, Zarrouki B, Tremblay C, Mancini AD, Maachi H, et al. The regulator of G-protein signaling RGS16 promotes insulin secretion and beta-cell proliferation in rodent and human islets. *Mol Metab.* 2016;5(10):988-96.

19. Kelso TWR, Porter DK, Amaral ML, Shokhirev MN, Benner C, and Hargreaves DC. Chromatin accessibility underlies synthetic lethality of SWI/SNF subunits in ARID1A-mutant cancers. *Elife.* 2017;6.

20. Bind MA, Lepeule J, Zanobetti A, Gasparrini A, Baccarelli A, Coull BA, et al. Air pollution and gene-specific methylation in the Normative Aging Study: association, effect modification, and mediation analysis. *Epigenetics.* 2014;9(3):448-58.

21. Chen R, Meng X, Zhao A, Wang C, Yang C, Li H, et al. DNA hypomethylation and its mediation in the effects of fine particulate air pollution on cardiovascular biomarkers: A randomized crossover trial. *Environ Int.* 2016;94:614-9.

22. Li H, Chen R, Cai J, Cui X, Huang N, and Kan H. Short-term exposure to fine particulate air pollution and genome-wide DNA methylation: A randomized, double-blind, crossover trial. *Environ Int.* 2018;120:130-6.

Figures

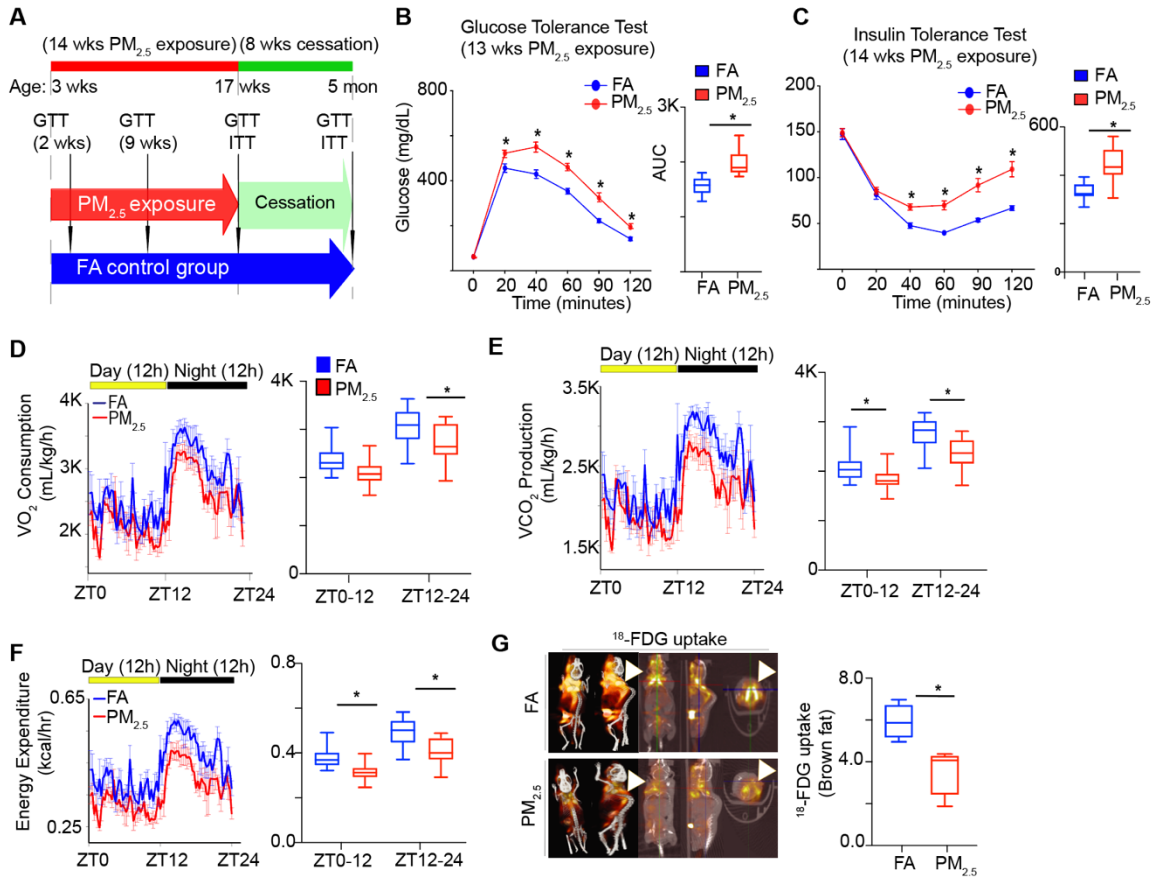

Fig. 1. Systemic effects of ambient air pollution ($PM_{2.5}$) on insulin resistance. (A) Experimental plan including a cessation period of 8 weeks following 14 weeks of FA or $PM_{2.5}$. (B) Glucose tolerance test (intraperitoneal administration of glucose (2g/kg body weight) and area under curve (AUC) (n=12/group). (C) Insulin tolerance test (intraperitoneal administration of insulin (0.75U/kg body weight) and AUC calculated (n=12/group). (D) VO_2 consumption (E) VCO_2 production and (F) EE. Line graphs indicate averages of day and night cycles over a 48h period, bar graphs indicate the total value at the time points indicated (n=6). (G) representative PET image (whole body FDG uptake) from FA and $PM_{2.5}$ exposed mice (n=4/group) and quantitative measurement of FDG uptake from brown adipose tissue (value of ROI). Data are expressed as mean ± SEM and *p<0.05 relative to FA mice as determined using a student's t-test or, where appropriate, a two-way analysis of variance (ANOVA).

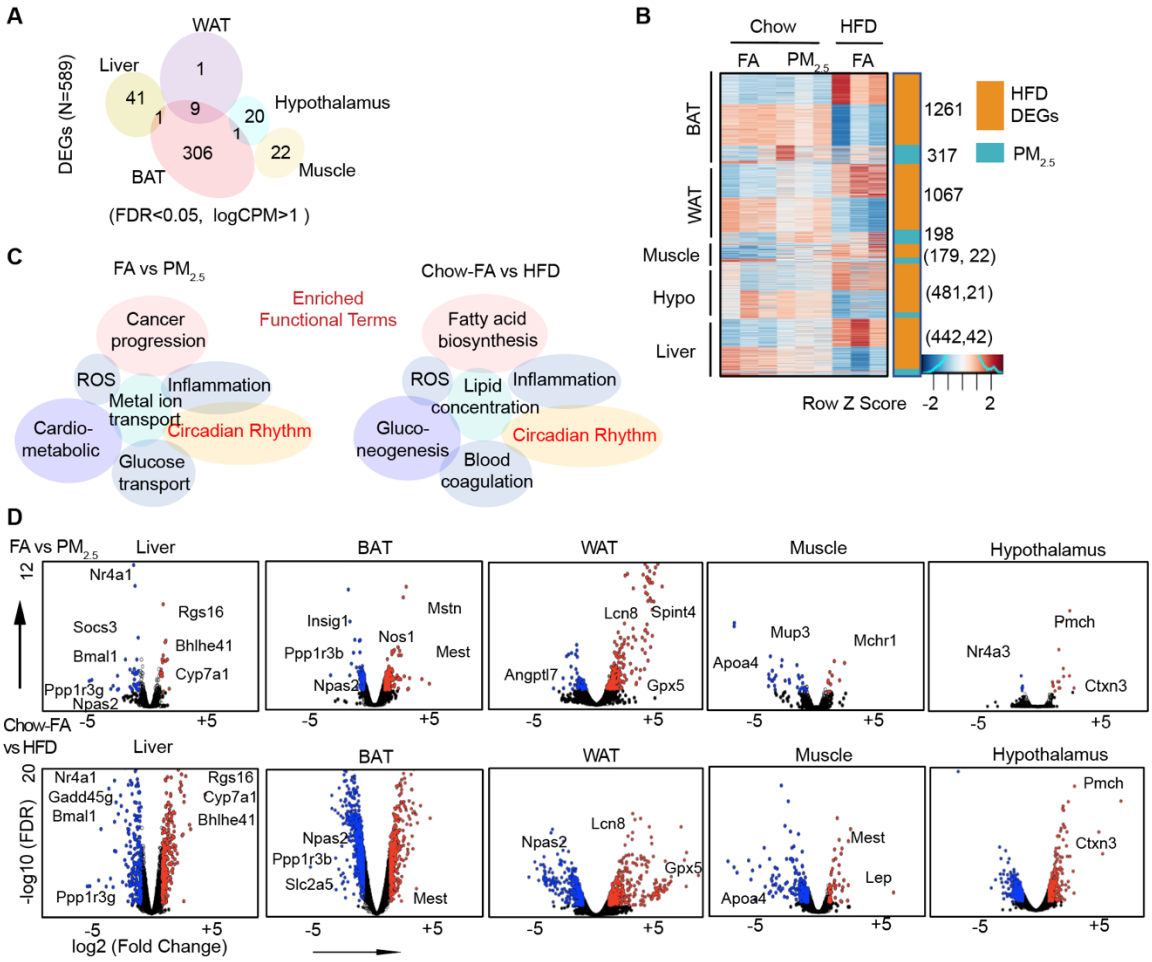

Fig. 2. Comprehensive transcriptome analysis in insulin response tissues. (A) Venn diagram depicting differentially expressed genes (DEGs) in various tissues from FA, and $PM_{2.5}$ exposed mice (FDR<0.05, logCPM>1). (B) Tissue specific DEGs and overlapped genes in FA, $PM_{2.5}$ and HFD mice (n=45). (C) The summary of enriched GO term and functional pathways in FA, $PM_{2.5}$ and HFD transcriptome. (D) Volcano plots comparing Chow *vs.* HFD and FA *vs.* $PM_{2.5}$ indicating selected DEGs of IR and stress response elements in various tissue from HFD fed mice.

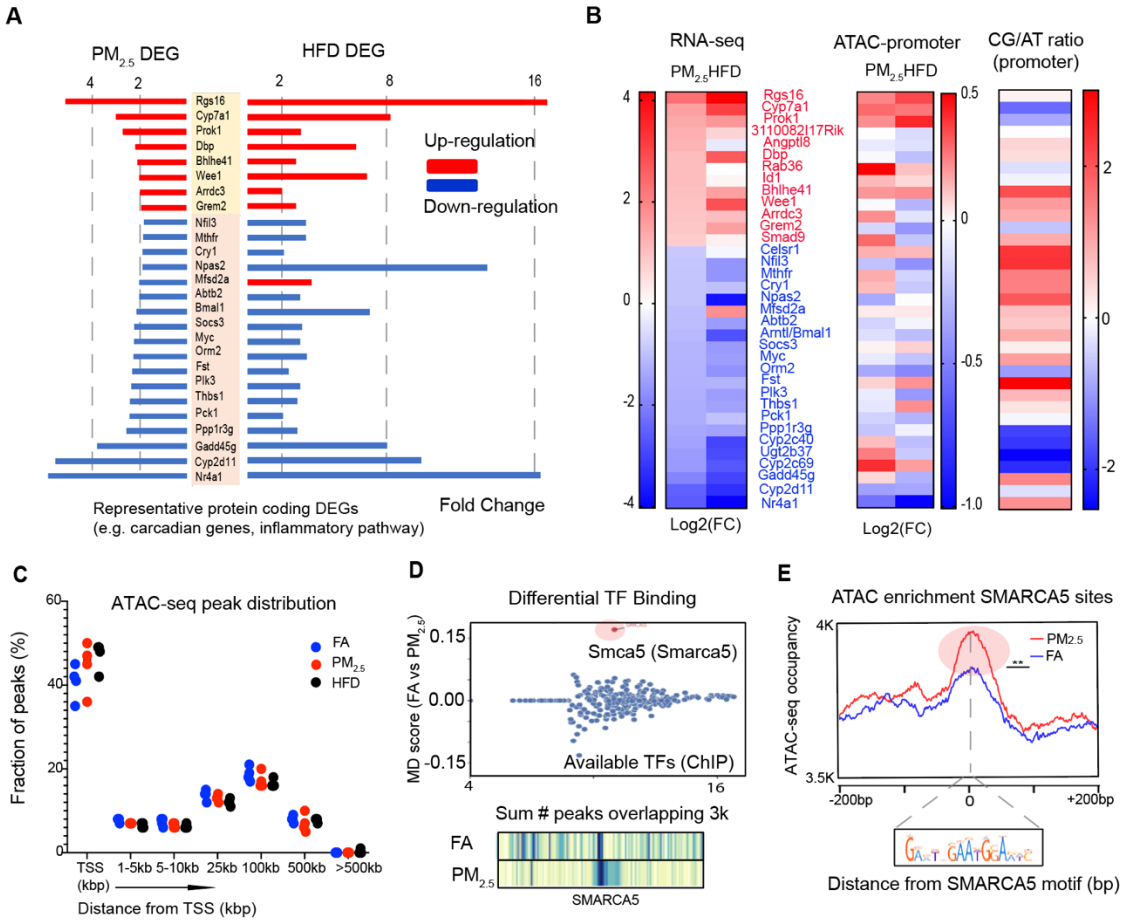

Fig. 3. Liver transcriptomic and epigenomic changes. (A) Comparison of the expression levels of DEGs (enriched inflammatory and circadian genes) between $PM_{2.5}$ and HFD. (B) Integrative analysis using RNA-seq and ATAC-seq datasets, and corresponding CpG content in promoters. (C) Open chromatin distribution across the three groups (FA, $PM_{2.5}$, and HFD) (D) Differential transcription factor binding analysis using available ChIP-seq database. (E) ATAC-seq enrichment on the SMARCA5 binding motifs.

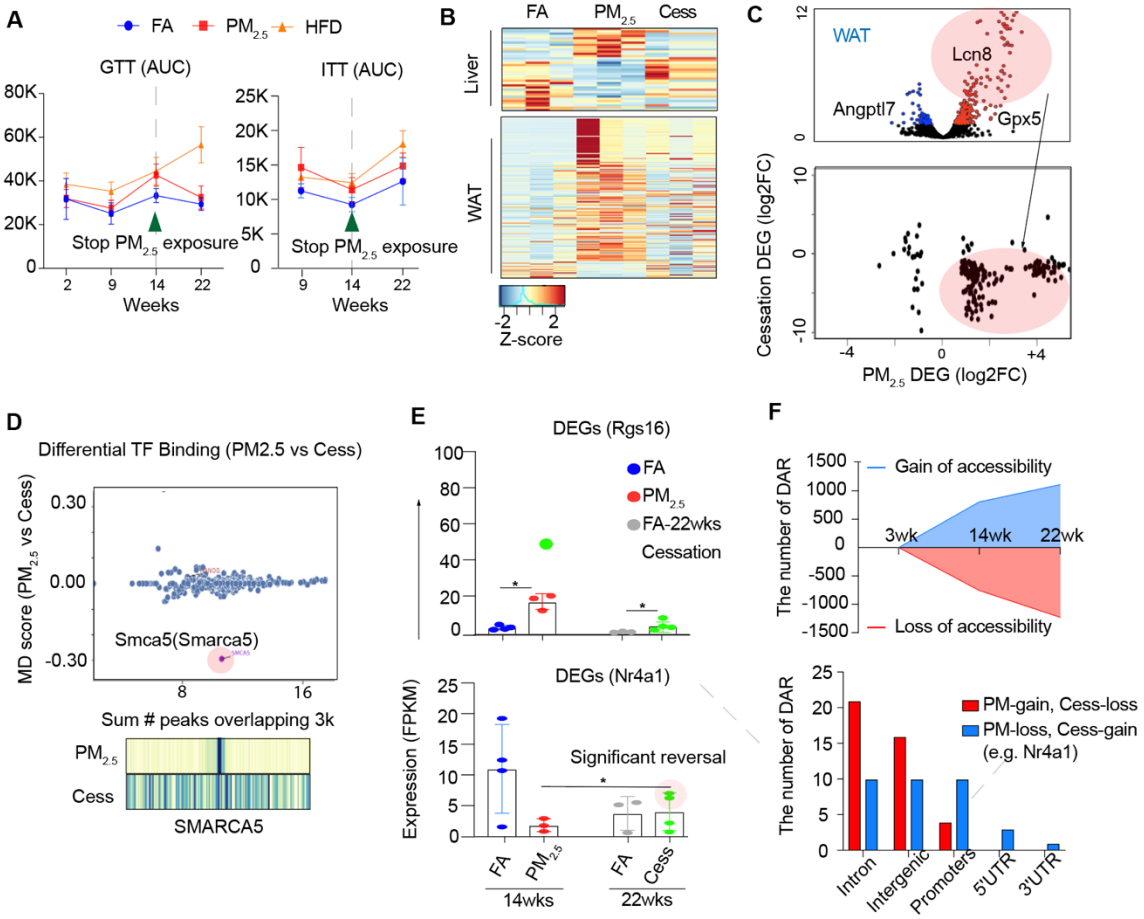

Fig. 4. Impact of exposure cessation *vs.* continued $PM_{2.5}$ exposure in liver. (A) Comparison of GTT and ITT, as represented by AUC, in FA, $PM_{2.5}$ and HFD mice at indicated time points, hashed line indicates cessation of exposure at 14 wks. (B) Heatmap of liver, and WAT DEGs upon 8-week $PM_{2.5}$ cessation (14-22 wks). (C) Volcano plot of 14wks WAT transcriptome, and scatter plot of DEG fold change distribution (x-axis: $PM_{2.5}$ DEG, y-axis: Cessation DEG), showing reversal of highly-upregulated genes in $PM_{2.5}$ (D) Differential TF binding analysis using ATAC-seq datasets and the reversal of SMARCA5 binding profiles ($PM_{2.5}$ *vs.* Cessation). (E) Quantitative assessment summarizing normalized transcript values for two select genes (Rgs16 and Nr4a1) across mice samples. (F) The summary of reversable differentially accessible regions (DAR) and genomic regions.